Part II: Monte Carlo Simulations

$$E = \frac{1}{2}\sum_{p,q} N_p^q J_p^q$$

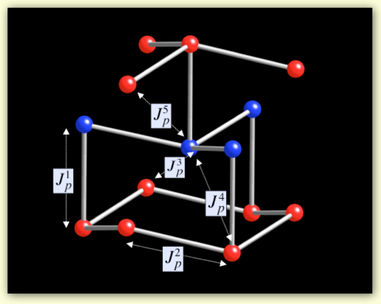

Fig. 10. Chemical exchange parameters define the excess energy due to Fe^{2+}-Fe^{3+}, Fe^{2+}-Ti, and Fe^{3+}-Ti nearest neighbours

$$E = -J_E \sum_{\langle i,j \rangle} \vec{S}_i \cdot \vec{S}_j$$

S_i

S_j

Fig. 11. Magnetic ordering is treated using an Ising-like approach. Fe cations are assigned a spin (either left or right), and the magnetic energy is calculated using a set of magnetic exchange parameters.

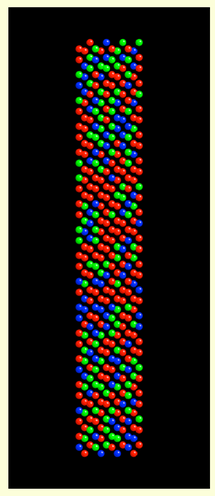

Fig. 12. A supercell of the hematite structure is created and a starting configuration of cations and spins is chosen. During the simulation, pairs of cations are chosen at random and their positions swapped. Alternatively, a single cation is chosen and its spin is flipped. If the energy change is negative then the swap is accepted. If the energy change is positive, the swap is accepted with a probability exp(-ΔE/RT).

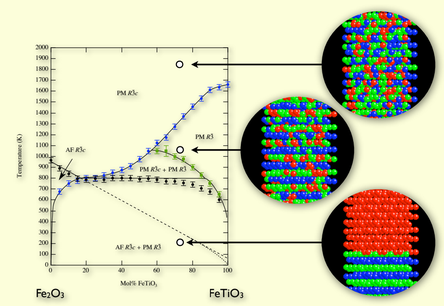

Fig. 13. A combination of cation swaps and spin flips is used to allow the system to reach its equilibrium degree of cation and magnetic order. To study magnetic ordering only, we keep the cation configuration fixed and allow only spin flips to occur.

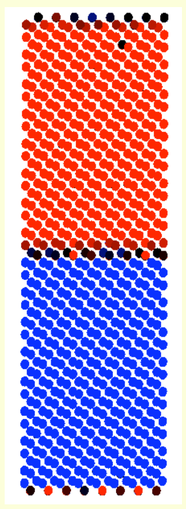

Fig. 14. An 8x8x8 supercell was initiated with bulk composition ilm70 and a fully ordered cation distribution. The positions of Fe and Ti cations in one half of the supercell were interchanged. This leads to a starting configuration containing an ordered (red) and an antiordered (blue) domain, separated by an antiphase domain boundary (black).

Fig. 15 (below left)
Annealing at 850 K (within the miscibility gap) leads to two equally well ordered and antiordered APDs separated by cation disordered APBs. Fig. 15a shows the distribution of Fe3+ (red), Fe2+ (green), and Ti (blue). Fig. 15b shows the degree of cation order (red = ordered, blue = antiordered). The APBs are enriched in Fe relative to the APDs (intensity of colour in Fig. 15c is proportional to the concentration of hematite). The distribution of left (blue) and right (red) spins (Fig. 15d) shows that the APDs are ferrimagnetic and the APBs are antiferromagnetic. The net moments of the ferrimagnetic APDs are equal and opposite.

Fig. 16 (below right)
Annealing at 1100 K (above the miscibility gap) leads to a reduction in the size and the degree of order in one APD (Fig. 16b). This happens as the system attempts to increase the degree of long-range order. Fe enrichment now occurs over the entire upper region of the supercell, encompassing both the APB regions and the poorly-ordered APD (Fig. 16c). The magnetic structure of the Fe-enriched region is close to being antiferromagnetic (Fig. 16d) but has a small ferrimagnetic moment due to the presence of the poorly cation ordered APD. This weak ferrimagnetic moment is opposite in sign to the large ferrimagnetic moment of well cation ordered

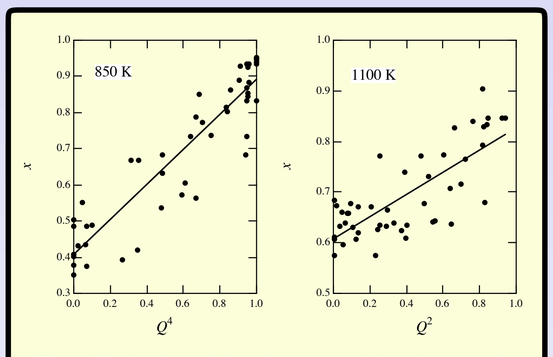

Fig. 17. A plot of local composition (x = mole fraction ilmenite) versus local degree of cation order from simulations below and above the miscibility gap. Both cases show positive correlation, illustrating that regions of poor cation order will be Fe enriched.

Fig. 15. Annealed at 850 K (below the miscibility gap)

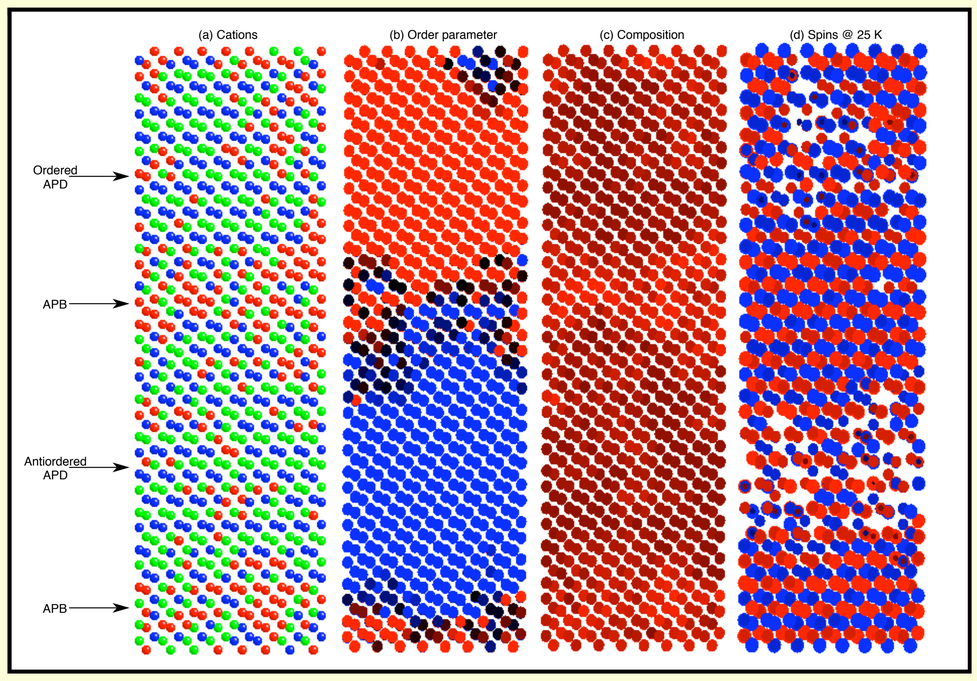

Fig. 16. Annealed at 1100 K (above the miscibility gap)

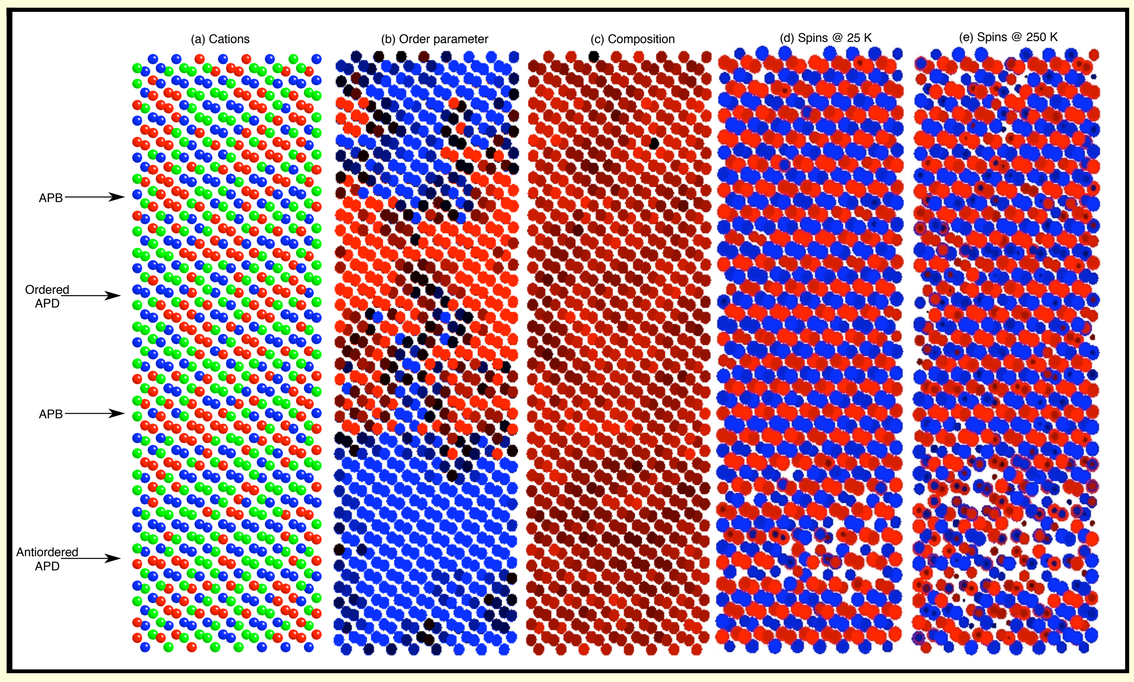

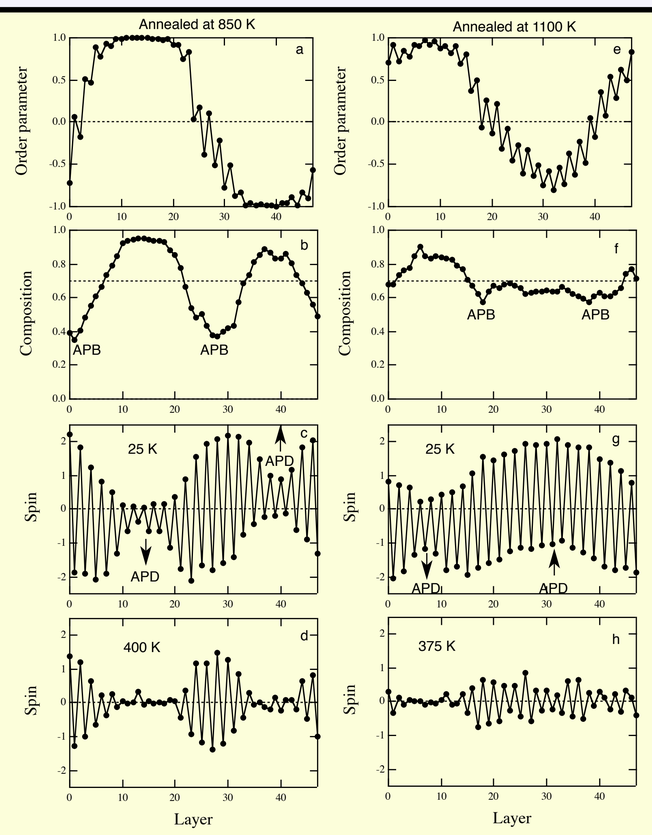

Fig. 18. Average values of order parameter, composition, and spin on each of the 48 layers of an 8x8x8 supercell pre-annealed at (a-d) 850 K (see Fig. 15) and (e-h) 1100 K (see Fig. 16). (a) The order parameter profile at 850 K shows two fully ordered/ antiordered APDs (Q = 1 and Q = -1, respectively) separated by APBs (Q = 0). (b) The composition profile at 850 K shows the cation disordered hematite-rich phase coinciding with the APBs. (c) The spin profile at 25 K shows that the APDs are strongly ferrimagnetic. The APD centred on layer 14 has a net negative spin, whereas the APD centred on layer 40 has a net positive spin (indicated by the arrows). (d) The spin profile at 400 K shows that the Fe-rich APBs remain magnetically ordered, whereas the Fe-poor APDs are magnetically disordered. The APBs are associated with a small net spin (see Fig. 19). (e) The order parameter profile at 1100 K shows a fully ordered APD ($Q \sim 1$) and a less well (anti)ordered APD ($Q \sim -0.75$). (f) The composition profile at 1100 K shows that the well ordered APD has x > 0.7, whereas the less well ordered APD has x < 0.7. Evidence for Fe enrichment at the APBs is also seen. (g) The spin profile at 25 K shows that the well ordered APD is strongly ferrimagnetic, whereas the ferrimagnetic spin of the less well ordered APD is decreased by the influence of the boundary regions. (h) The spin profile at 375 K shows that the less well ordered APD and boundary regions are magnetically ordered, whereas the well ordered APD is magnetically disordered.The magnetically ordered regions carry a small net spin that is opposite to the net spin of the well ordered APD (see Fig. 14).

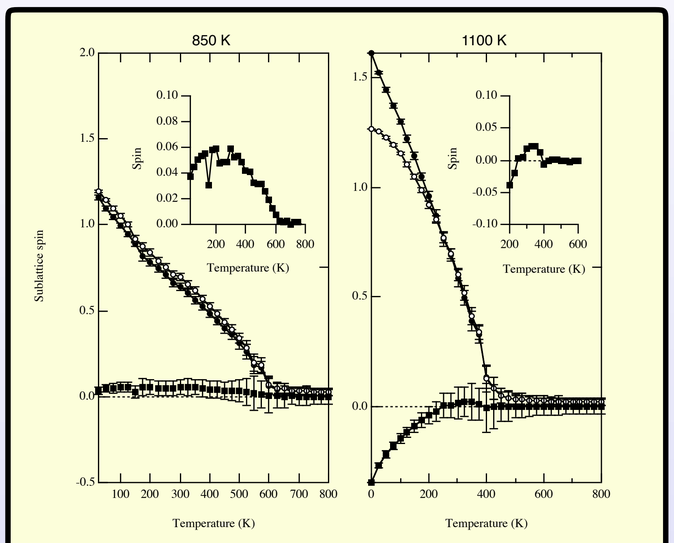

Fig. 19. Sublattice spins and net magnetisation as a function of temperature. The 850 K microstructure (a) has a small net moment and no self reversal. The 1100 K microstructure (b) is ferrimagnetic at low temperature, and displays a self reversal of the net magnetisation.

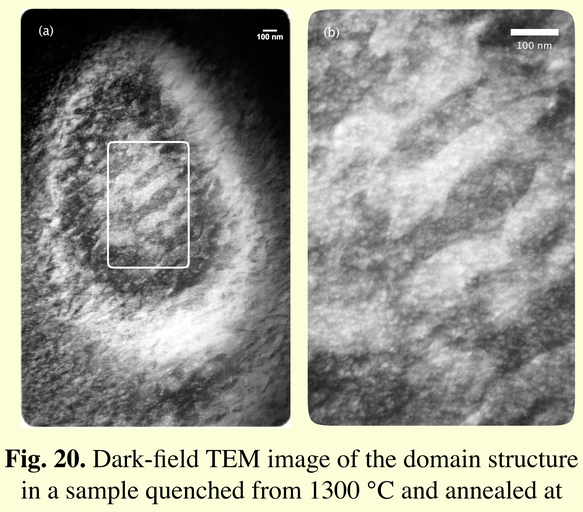

Fig. 20. Dark-field TEM image of the domain structure in a sample quenched from 1300 °C and annealed at 650 °C for 10 hours. The microstructure consists of fine scale heterogeneities (~4-8 nm diameter spots with spacing ~10-20 nm) superimposed on larger-scale (~100 nm wide) APDs. The microstructure is consistent with the mechanism of transformation from short- to long-range cation order proposed in Fig. 21d.

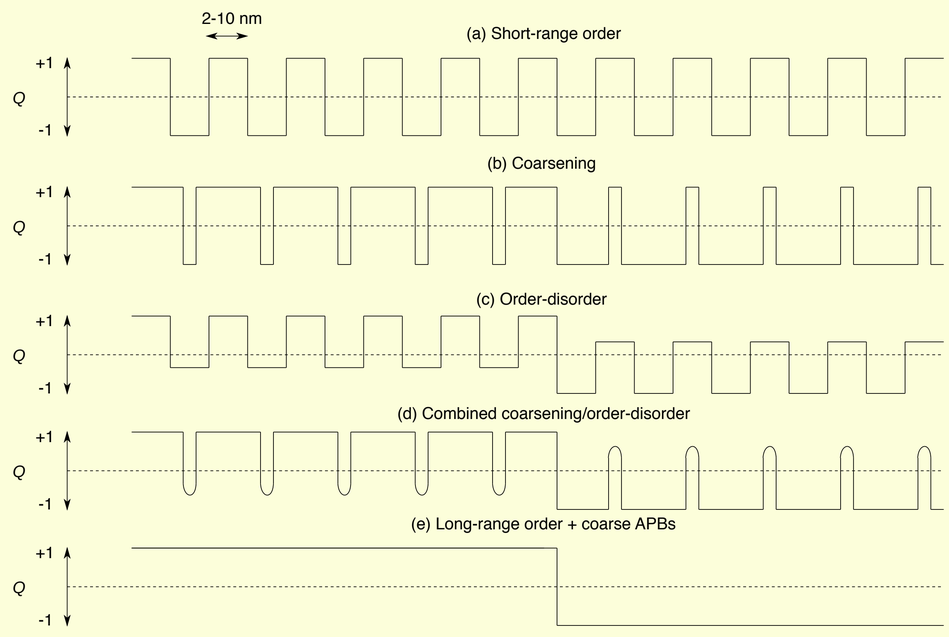

Fig. 21. Schematic illustration of the transition from (a) short-range to (e) long-range cation order via a (b) coarsening, (c) order-disorder, and (d) combined mechanism. **Only the combined mechanism will generate self-reversed TRM**. The left and right hand sides of the diagrams correspond to large-scale antiphase domains with opposite net magnetisation. Negative exchange coupling across the central APB can be easily overcome, however, by the formation of a 0° wall.